Lattice dynamics of BC_2N

Hanae Nozaki and Satoshi Itoh
Advanced Research Laboratory, Toshiba Corporation, 1 Komukai Toshiba-cho, Saiwai-ku, Kawasaki 210, Japan
(Received 18 December 1995)

A layered material, BC_2N, has huge polymorphic structures which depend on the atomic arrangements. In order to investigate the relation between the vibrational properties of monolayer BC_2N systems and their intralayer atomic arrangements, the lattice vibrations of various polymorphic structures are calculated based on a generalized valence-force field model whose force constants have been determined from *ab initio* total energy calculations. The obtained phonon density-of-states spectra, phonon dispersion relations, and vibrational modes are presented and discussed in detail. As for BC_2N systems with homogeneous atomic arrangements, their vibrational modes with higher frequencies are sensitively influenced by local atomic arrangements, and give different peak structures in the phonon spectra. In contrast, as for BC_2N systems with patterns segregated into graphitelike and hexagonal boron nitridelike regions, if each segregated domain contains more than dozens of atoms, their phonon spectra can be described by a superposition of the spectra of graphite and hexagonal boron nitride. The analysis of the lattice vibrations of BC_2N has a possibility of leading to the determination of its polymorphic structures. [S0163-1829(96)01421-X]

I. INTRODUCTION

Quite recently, interest has been growing in a B-C-N layered material family, and its several stoichiometric compounds such as BC_xN with $x=2$, 3, and 5 have been synthesized by means of the chemical vapor deposition method.[1,2] These materials have graphitic structures in which some carbon atoms are substituted with boron and/or nitrogen atoms, so that it is characteristic of B-C-N layered materials to show the charge transfer between atoms in intralayers. As compounds based on graphitic structures, graphite intercalation compounds (GIC's) are well known, and their characteristics are attributed to a weak interlayer interaction of graphite derived from nonbonding van der Waals interactions. There are both donor-type and acceptor-type GIC's, because of the intermediate value of electronegativity of carbon atoms. In these GIC's, the charge transfer occurs between intercalant layers and graphite sheets, and the intercalation technique is one of the methods to control the electronic properties of layered materials. In contrast to GIC's, B-C-N layered materials show the charge transfer in intralayers, and therefore can be expected to open a new possibility of controlling electronic properties.

In the B-C-N family, BC_3 and BC_2N are well studied experimentally,[1,2] and several theoretical investigations of BC_2N respecting the equilibrium structures,[3,4] the electronic properties,[3,5] and the vibrational properties[6,7] have been reported recently. This material, BC_2N, has huge polymorphic structures which depend on the atomic arrangements. However, their detailed crystal structures, even their lattice constants, have not yet been determined experimentally, because of the difficulty of synthesizing high quality crystals. The relation between the structural stability of BC_2N and its atomic arrangements has been comprehensively investigated based on a semiclassical method, and it is expected that the stable structure of BC_2N is such that as many C-C and B-N bonds as possible are formed.[4] It has also been theoretically suggested that the electronic properties of this material sensitively change depending on local atomic arrangements in intralayers.[3,5]

It is the purpose of the present paper to investigate the relation between the lattice vibrations and the intralayer atomic arrangements of BC_2N. As polymorphic structures of BC_2N, both small-sized and large-sized unit cell models are taken into account. Their phonon density-of-states (DOS) spectra, phonon dispersion relations, and vibrational modes have been calculated and analyzed in detail. In this study, a generalized valence-force field model is adopted as the interatomic potential of BC_2N, and its force constants have been determined from *ab initio* total energy calculations.

This paper is organized as follows. In the next section, structural models of BC_2N are presented, and, in Sec. III, the interatomic potential of this material and its potential parameters are described. In Sec. IV, the calculated vibrational properties of BC_2N are reported in detail. The obtained numerical results for the small-sized and the large-sized unit cell models are discussed, and they are also compared with the lattice vibrations of graphite and hexagonal boron nitride (h-BN). Finally, a short summary is given in Sec. V.

II. STRUCTURAL MODELS

Before discussing the vibrational properties of BC_2N, let us briefly summarize its structural properties which have been described in detail in elsewhere.[4] In that study, the structural stability of BC_2N depending on the atomic arrangements has been investigated from the viewpoint of a simple bond energy accounting. Only a monolayered model has been considered there, because interlayer interactions of BC_2N originating from nonbonding van der Waals interactions are expected to be weaker than covalent intralayer interactions. In layered materials, their various properties such as lattice vibrations are primarily influenced by atomic arrangements in intralayers, and thus the monolayered structural model is also adopted in this study.

Five typical polymorphic structures of BC_2N are shown in

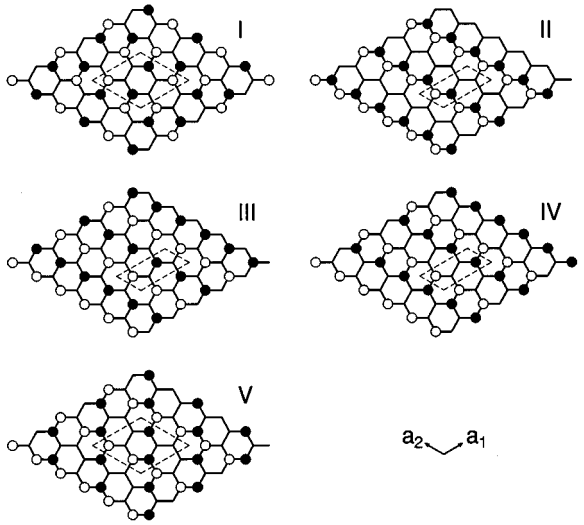

FIG. 1. Crystal structures of BC_2N with homogeneous atomic arrangements, where open and closed circles indicate B and N atoms, respectively, and C atom is located at each vertex point. Dashed lines show unit cells containing 4 or 8 constituent atoms.

Fig. 1. These structures have four or eight constituent atoms in their unit cells, and show relatively well-mixed arrangements of the three elements: B, C, and N. In such ''homogeneous'' BC_2N systems, their honeycomb lattices are constituted of different combinations of chemical bonds: C-C, B-N, B-C, C-N, B-B, and N-N. The structural characteristics of the five models in Fig. 1 are as follows: model I has the highest symmetry among all polymorphic structures of BC_2N, models II–IV have quasi-one-dimensional structures composed by parallel zigzag chains, and model V has an almost random atomic arrangement.

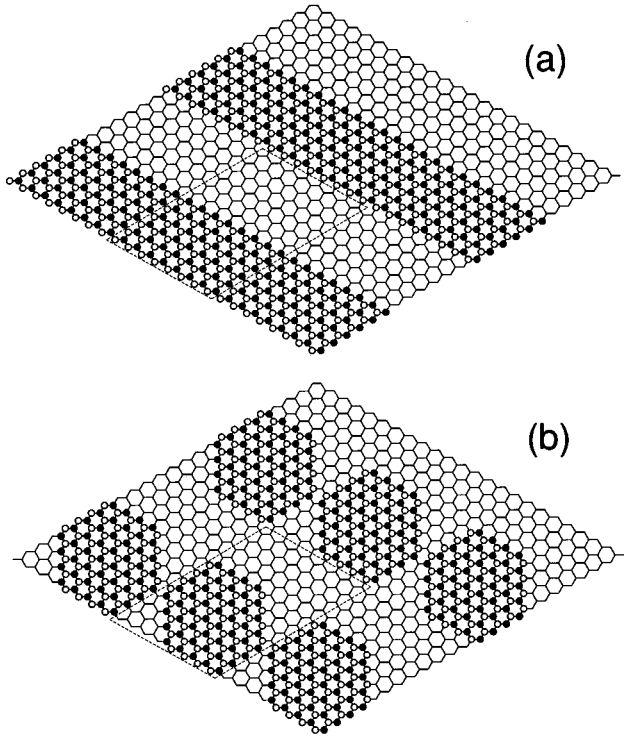

FIG. 2. Crystal structures of BC_2N with largely segregated patterns: the striped (a) and the island (b) patterns whose unit cells contain 192 atoms.

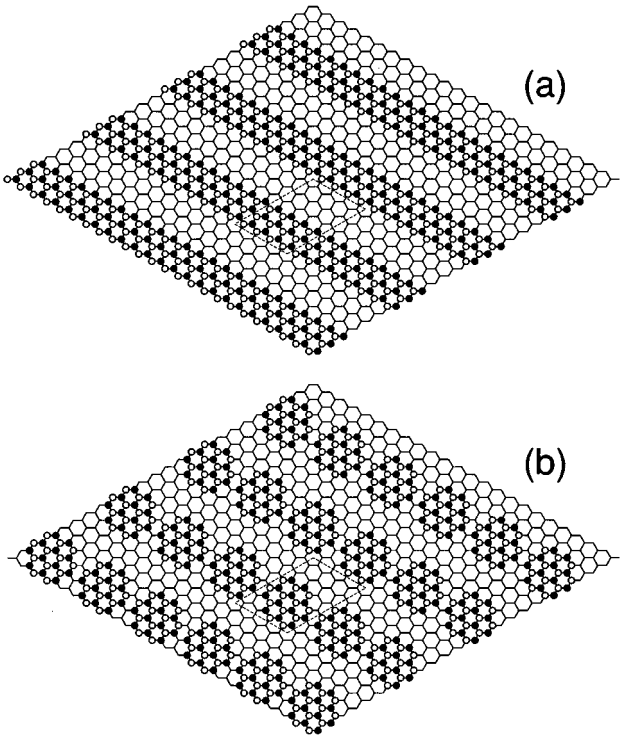

FIG. 3. Crystal structures of BC_2N with segregated patterns: the striped (a) and the island (b) patterns whose unit cells contain 48 atoms.

It is possible to roughly estimate the cohesive energies of BC_2N systems based on the chemical bond energies. By using this semiclassical method, it has been found that model II, which has parallel zigzag -C-C- and -B-N- chains, is the most stable structure among all homogeneous BC_2N systems, because this model has the most C-C and B-N bonds whose bond energies are larger than those of the other chemical bonds. This result, which is also supported by *ab initio* calculations,[3,8] implies that the stable structure of BC_2N is such that the number of both C-C and B-N bonds is increased, which means there is a possibility of the existence of BC_2N systems with phase separations into graphitelike and *h*-BN-like regions.

As such ''segregated'' BC_2N systems, there are two possible segregated patterns: the striped and the island ones given in Figs. 2 and 3. In the case of the island patterns, each segregated domain in Figs. 2(b) and 3(b) contains 96 and 24 atoms, respectively. Based on the semiclassical method, the following results have been obtained: with increasing the size of segregated domains, the cohesive energies per atom become large, because of the increase in the number of C-C and B-N bonds. In the segregated systems, B-C and C-N bonds which have smaller bond energies than C-C and B-N bonds are located only in the boundaries between the two kinds of phases. If the size of segregated patterns is relatively small, the striped pattern is more stable than the island one,

because these two patterns show a large difference in the number of B-C and C-N bonds. However, when the size of segregated patterns is large enough, the difference between the cohesive energies of the two patterns becomes negligibly small. As mentioned above, the most stable structure among the homogeneous BC_2N systems is model II given in Fig. 1, and this structure corresponds to the striped pattern with the narrowest width.

In this study, the lattice vibrations of both the homogeneous and the segregated BC_2N systems are calculated. By comparing those numerical results, the influence of intralayer atomic arrangements upon the vibrational properties of BC_2N will be discussed in Sec. IV.

III. INTERATOMIC POTENTIAL

The use of empirical models is required in the present calculation for BC_2N, because it is difficult to treat large-sized systems, such as the above-mentioned segregated systems, by using *ab initio* calculations. Since the interatomic interaction in intralayers of BC_2N mainly originates from the covalent bonds, it is reasonable to adopt a generalized valence-force field model. In this model, the total potential energy is given by the following expression:

$$E_{\text{total}}=\sum_{ij}\ \frac{1}{2}K^{ij}_{r_{(1)}}(r^{ij}_{(1)}-\overline{r}^{ij}_{(1)})^2+\sum_{ij}\ \frac{1}{2}K^{ij}_{r_{(2)}}(r^{ij}_{(2)}-\overline{r}^{ij}_{(2)})^2+\sum_{ijk}\ \frac{1}{2}K^{ijk}_{\theta}(\theta^{ijk}-\overline{\theta^{ijk}})^2+\sum_{ijkl}\ \frac{1}{2}K^{ijkl}_{\phi}[1-\cos\{2(\phi^{ijkl}-\overline{\phi^{ijkl}})\}], \quad (1)$$

where the four terms correspond to bond stretching, second bond stretching, bond bending, and torsion energies.

The potential parameters of the first three terms in Eq. (1), the force constants $K_{r_{(1)}}$, $K_{r_{(2)}}$, and K_θ and the equilibrium bond lengths $\overline{r}_{(1)}$ and $\overline{r}_{(2)}$, are determined from *ab initio* total energy calculations based on the Hartree-Fock method. Since four kinds of chemical bonds (C-C, B-N, B-C, and C-N) exist in the crystal structures shown in Figs. 1–3, these *ab initio* calculations have been carried out for monolayer graphite, *h*-BN, *h*-BC, and *h*-CN, where the last two materials have not been obtained experimentally. The charge transfer between B, C, and N atoms occurs in the last three materials: *h*-BN, *h*-BC, and *h*-CN. This effect is reflected in the potential parameters of Eq. (1), because the charge distribution has been determined self-consistently in the electronic calculations. Thus, as the first approximation, it could be considered that the present generalized valence-force field model takes into account some effect of the intralayer charge transfer in BC_2N systems.

In this study, our attention is focused on the lattice vibrations whose vibrational vectors are parallel to layers, because such vibrational modes are strongly influenced by the atomic arrangements in intralayers. In Eq. (1), the first three terms contribute to the vibrational modes having in-plane displacement vectors, but the last term giving torsion energy contributes only to the vibrational modes whose displacement vectors are perpendicular to the planes. Therefore, the force constant K_ϕ is determined so as to agree with the experimental dispersion curves of graphite whose vibrational modes have out-of-plane displacement vectors. The obtained potential parameters are given in Table I. In the calculations of lattice vibrations, all crystal structures have been optimized based on the present generalized valence-force field model. And, it has been ascertained that model II is the most stable among the five models I–V having the optimized crystal structures.

TABLE I. Potential parameters of BC_2N in the generalized valence-force field model, where symbol X indicates any one of three elements: B, C, and N.

	Bond stretching			Second bond stretching	
	$K^{ij}_{r_{(1)}}$	$\overline{r}^{ij}_{(1)}$		$K^{ij}_{r_{(2)}}$	$\overline{r}^{ij}_{(2)}$
i-j	(eV/Å^2)	(Å)	i-k-j	(eV/Å^2)	(Å)
B-C	9.351	1.598	C-B-C	4.783	2.768
B-N	13.070	1.475	N-B-N	4.783	2.555
C-C	14.334	1.463	B-C-B	5.676	2.768
C-N	15.236	1.433	C-C-C	5.676	2.534
			N-C-N	5.676	2.482
			B-N-B	10.549	2.555
			C-N-C	10.549	2.482
	Bond bending			Torsion	
	K^{ijk}_{θ}	$\overline{\theta^{ijk}}$		K^{ijkl}_{ϕ}	$\overline{\phi^{ijkl}}$
i-j-k	(eV/rad^2)	(rad)	i-j-k-l	(eV)	(rad)
X-B-X	3.591	$2\pi/3$	X-X-X-X	1.030	0 or π
X-C-X	7.716	$2\pi/3$			
X-N-X	9.561	$2\pi/3$			

In order to check the validity of Eq. (1) and its potential parameters, the lattice vibrations of monolayer graphite and *h*-BN have been calculated. The calculated phonon dispersion relation of monolayer graphite is shown in Fig. 4 together with the experimental dispersion curves.[9,10] Because of the weak interlayer interactions of graphite derived from van der Waals interactions, there is no notable difference between the dispersion relations calculated based on the monolayered and the multilayered models, except for branches with low frequencies of about 100 cm^{-1} around the Γ point which concern the acoustic modes in the monolayered model. From Fig. 4, it has been found that the phonon dispersion relation of monolayer graphite calculated by using Eq. (1) is in fairly good agreement with the experimental ones. The calculated phonon frequencies at the Γ point are 886 and 1563 cm^{-1}, where the former is assigned to B_{1g} and A_{2u} modes and the latter is assigned to E_{2g} and E_{1u} modes for three-dimensional crystal graphite (the space group is D^4_{6h}). Their experimental data by means of Raman scattering or infrared (IR) absorption are 868 cm^{-1} (A_{2u}), 1581 cm^{-1} (E_{2g}), and 1587 cm^{-1} (E_{1u}).[11,12] The space group of *h*-BN is also D^4_{6h}, and its irreducible representations at the Γ point are the same as those of graphite. The calculated phonon frequencies of monolayer *h*-BN at the Γ point are 812 and 1444 cm^{-1}, and they are also in good agreement with the corresponding experimental data of 780 cm^{-1} (A_{2u}), 1366 cm^{-1} (E_{2g}), and 1390 cm^{-1} (E_{1u}).[13,14]

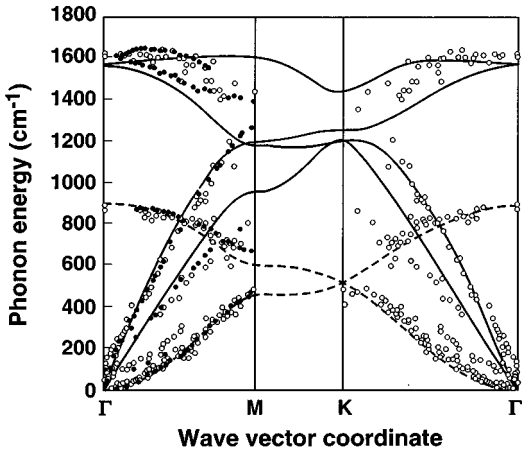

FIG. 4. The calculated phonon dispersion relation of monolayer graphite, where solid and dashed lines show the vibrational modes with in-plane and out-of-plane displacement vectors, respectively. Closed and open circles indicate experimental data by means of electron energy loss spectroscopy by Oshima *et al.* (Ref. 9) and Wilkes *et al.* (Ref. 10), and the latter data are plotted along both the $\Gamma-M$ and the $\Gamma-K$ directions, because of the use of highly oriented pyrolitic graphite.

IV. LATTICE VIBRATIONS

In this section, the obtained numerical results for the vibrational properties of the homogeneous and the segregated BC_2N systems are presented. Since it has been found that these two systems show quite different vibrational characteristics, they are discussed in separate subsections.

A. Homogeneous systems

1. Phonon density-of-states spectra

The calculated phonon DOS spectra of the homogeneous BC_2N systems (models I–V) are shown in Fig. 5. These phonon spectra have been calculated with 2401 **q** points in the whole Brillouin zone (BZ), and each vibrational level has been broadened with Gaussian functions of the full width at half maximum of 33.3 cm^{-1}, where the two-dimensional BZ is given in Fig. 6. Here, it should be noted that the BZ's of

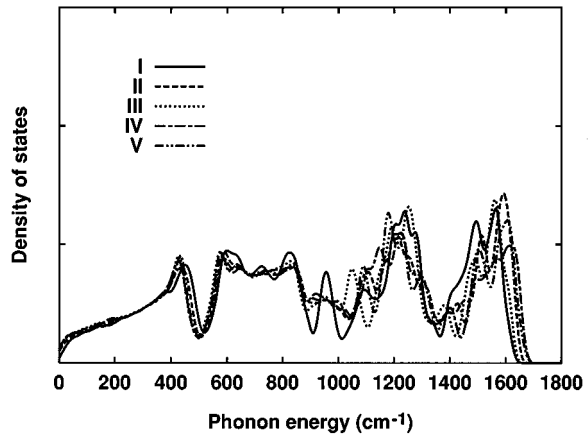

FIG. 5. The calculated phonon DOS spectra of the five homogeneous BC_2N systems shown in Fig. 1.

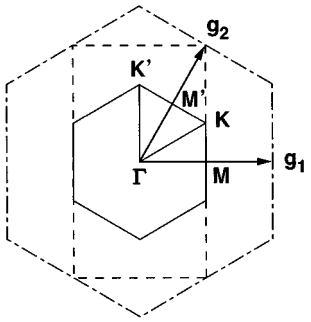

FIG. 6. Two-dimensional hexagonal Brillouin zone of BC_2N systems with 2×2 unit cells, where $\mathbf{g}_1$ and $\mathbf{g}_2$ indicate its reciprocal lattice vectors. Dashed and chain lines show rectangular Brillouin zone of 2×1 unit cells and hexagonal one of 1×1 unit cells, respectively.

models II–IV differ from those of models I and V. As compared with the two-dimensional 1×1 unit cell of monolayer graphite or *h*-BN, models II–IV have 2×1 unit cells and models I and V have 2×2 unit cells. As a result, the BZ's of models II–IV and models I and V have rectangular and hexagonal forms, respectively, as shown in Fig. 6. In order to compare the phonon dispersion relations of models II–IV with those of models I and V, 2×2 unit cells are also adopted for models II–IV in this study, and the hexagonal BZ of the 2×2 unit cell is used for all five models in Fig. 1.

In Fig. 5, the five phonon DOS spectra show different peak structures particularly in the higher energy region above 900 cm^{-1}. According to the analysis of their partial DOS's, the phonon spectra in this energy region are contributed only from the vibrational modes with in-plane displacement vectors. This means that the peak structures in the higher energy region reflect the difference in the intralayer atomic arrangements between models I–V. On the other hand, the peak structures in the lower energy region have little dependence on the polymorphic structures. We focus our attention on lattice vibrations whose energies are more than 900 cm^{-1}, hereafter.

Let us compare the lattice vibrations of the homogeneous BC_2N systems with those of graphite and *h*-BN, because graphite and *h*-BN can be regarded as prototype crystal structures of BC_2N. The calculated phonon DOS spectra of monolayer graphite and *h*-BN are shown in Fig. 7, together with a superposition of them. In this superposed spectrum of graphite and *h*-BN sheets, there are two peak structures in the higher energy region above 900 cm^{-1}: one is a broad peak centered at about 1200 cm^{-1} and the other is a sharp peak at 1600 cm^{-1}. Referring to the spectra of graphite and *h*-BN sheets, in the energy region where the former broad peak is located, a cancellation of the spectra of graphite and *h*-BN sheets can be seen. And, the latter sharp peak is mainly attributed to a graphitelike network, and its shoulder structure at 1680 cm^{-1} is derived from a *h*-BN-like network. In Fig. 7, the superposed spectrum shows a large difference in the intensity between those broad and sharp peak structures. Such two peak structures are also obtained in the phonon spectra of the homogeneous BC_2N systems given in Fig. 5: they are centered at about 1200 and 1550 cm^{-1}, where a peak of model I at about 950 cm^{-1} is regarded as an additional peak. However, the difference in the intensity between

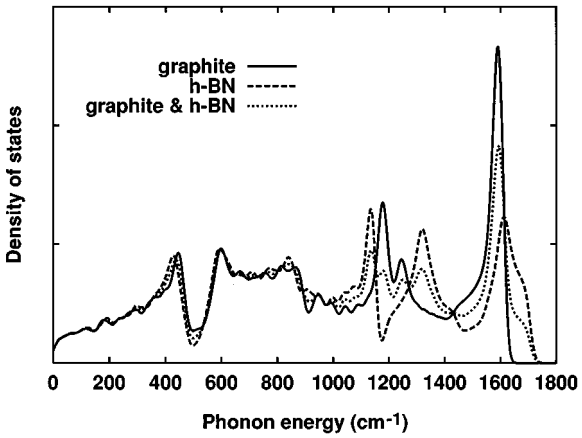

FIG. 7. The calculated phonon DOS spectra of monolayer graphite (solid line) and monolayer *h*-BN (dashed line), together with the superposition of them (dotted line).

these two peak structures is small in the case of the homogeneous BC_2N. Moreover, the sharp peak at 1600 cm^{-1} and the shoulder structure at 1680 cm^{-1}, which appear in the superposed spectrum of graphite and *h*-BN sheets, are not shown in the spectra of the homogeneous BC_2N. In Fig. 7, both the sharp peak of graphite and the shoulder structure of *h*-BN are derived from the LO mode. It has been found that the dispersion of the LO mode is largely contributed from the second bond stretching energy in Eq. (1) which well reflects the network structures. Since graphitelike and *h*-BN-like networks have disappeared in the homogeneous BC_2N systems, it is reasonable that the phonon spectra in Fig. 5 show neither such sharp peak nor shoulder structure in the higher energy region. From the above-mentioned viewpoints, it has been concluded that the lattice vibrations of the homogeneous BC_2N systems cannot be explained by the superposition of the spectra of monolayer graphite and *h*-BN, and that it is important to consider the contribution from B-C and C-N bonds which does not occur in graphite and *h*-BN.

In Fig. 5, there are no remarkable differences between the phonon DOS spectra of the homogeneous BC_2N systems, except for the peak of model I at about 950 cm^{-1}. However, we have found that their partial DOS spectra for the three elements (B, C, and N) show more obvious differences depending on the atomic arrangements. In particular, models I–V show characteristic peak structures in the partial DOS spectra for B and N atoms. These calculated spectra are presented in Fig. 8. On the other hand, in the partial DOS spectra for C atoms, the five models show peak structures which are quite similar to their own total DOS spectra given in Fig. 5. In order to investigate the contribution from B-C and C-N bonds to the lattice vibrations of BC_2N systems, the phonon spectra of monolayer *h*-BC and *h*-CN have also been calculated. As compared with the partial DOS spectra of monolayer graphite, *h*-BN, *h*-BC, and *h*-CN, the following have been found. First, in the partial DOS spectra for B atoms given in Fig. 8(a), models II and III have characteristic peaks at about 1600 and 1050 cm^{-1}, respectively. Referring to the partial DOS spectra of *h*-BN and *h*-BC sheets, the former and the latter peaks are attributed to vibrations of B atoms in *h*-BN sheet and in *h*-BC sheet, respectively. This is consistent with the fact that model II has the most B-N bonds and

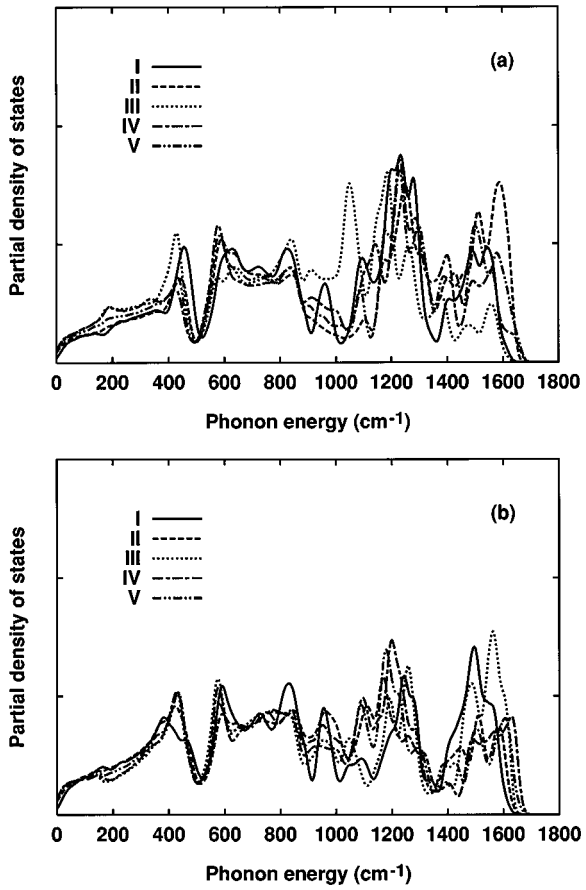

FIG. 8. The calculated partial DOS spectra of the homogeneous BC_2N systems given in Fig. 1: (a) for B atoms and (b) for N atoms.

model III has the most B-C bonds among the homogeneous BC_2N systems. Secondly, in the partial DOS spectra for N atoms given in Fig. 8(b), the peak structures above 1400 cm^{-1} of models I and III show higher intensity than the other models. Making a comparison between *h*-BN and *h*-CN sheets, vibrations of N atoms in *h*-CN sheet contribute more to the phonon spectrum in the higher energy region than those in *h*-BN sheet. Since models I and III involve more C-N bonds than the other models, it is reasonable that, in the partial DOS spectra for N atoms, models I and III show higher intensity in the energy region above 1400 cm^{-1}. Lastly, in a comparison between Figs. 8(a) and 8(b), only models II and V show higher intensity of the partial DOS spectra for B atoms than those of N atoms in the energy region above 1400 cm^{-1}. This is due to the fact that models II and V have the most and the second most B-N bonds among the five models, and vibrations of B atoms in *h*-BN sheet become more dominant than those of N atoms in the higher energy region.

In models II–V, there are two or four different types of C atoms. We have calculated the partial DOS spectra for each type of C atom, and found that these spectra depend on the kind of surrounding atoms. The calculated partial DOS spectra for four atom types [B, C(1), C(2), and N] of model II are shown in Fig. 9, where C(1) presents one which bonds to more B atoms than N atoms, and C(2) presents one which bonds to more N atoms than B atoms. In this figure, the spectra of C(1) and C(2) have the highest peak at about 1200

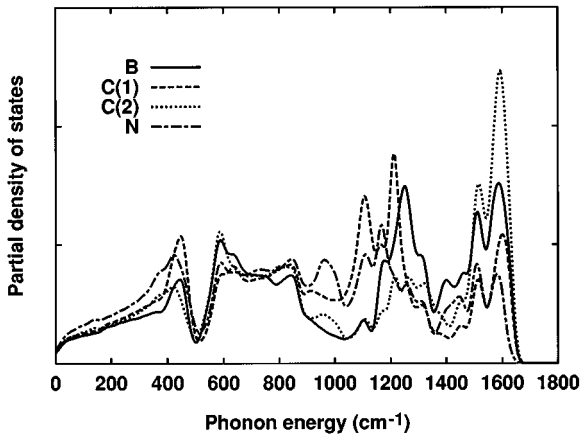

FIG. 9. The calculated partial DOS spectra of model II for the individual atom types: B, C(1), C(2), and N. See text for details.

and 1600 cm^{-1}, respectively. These peaks are attributed to the vibrations of C atoms in *h*-BC sheet and in *h*-CN sheet, respectively, referring to the partial DOS spectra of *h*-BC and *h*-CN sheets. As for all spectra in Fig. 9, we have found that their peak structures in the higher energy region are qualitatively described by weighted superpositions of the partial DOS spectra of monolayer graphite, *h*-BN, *h*-BC, and *h*-CN, where weighted factors are determined so as to be consistent with the number of chemical bonds (C-C, B-N, B-C, and C-N) in model II. Models III and IV also have four atom types: B, C(1), C(2), and N. It has been ascertained that, if the weighted factors are changed so as to be consistent with the number of chemical bonds in model III or IV, their partial DOS spectra in the higher energy region are also qualitatively described by the weighted superpositions. These results imply that the vibrational properties of BC_2N systems in the energy region above about 1000 cm^{-1} can be understood from the viewpoint of the kind and the number of chemical bonds, but are not strongly influenced by network structures of these chemical bonds, which is consistent with the fact that the bond stretching modes are more dominant than the bond bending modes in the higher energy region. However, it is difficult to explain the peak structures above 1600 cm^{-1} by such simple weighted superpositions, because they are contributed from the second bond stretching modes which depend on the network structures.

2. Phonon dispersion relations

In Fig. 5, a large difference between the five phonon spectra is caused by the peak structure of model I at about 950 cm^{-1}. To investigate the origin of this characteristic peak structure, we have compared the lattice vibration of model I with that of model II, because model II is the most stable structure among the homogeneous BC_2N systems. The calculated phonon dispersion relations of models I and II are shown in Fig. 10, where high symmetry points in the BZ are defined in Fig. 6. As mentioned previously, the BZ of the 2×2 unit cell is also used for model II, so that the dispersion relation of model II with the 2×1 unit cell shows double degeneracies at the M' point in Fig. 10(b). In Fig. 10(a), the dispersion relation of model I has a dispersiveless branch at about 950 cm^{-1} as compared with that of model II. This

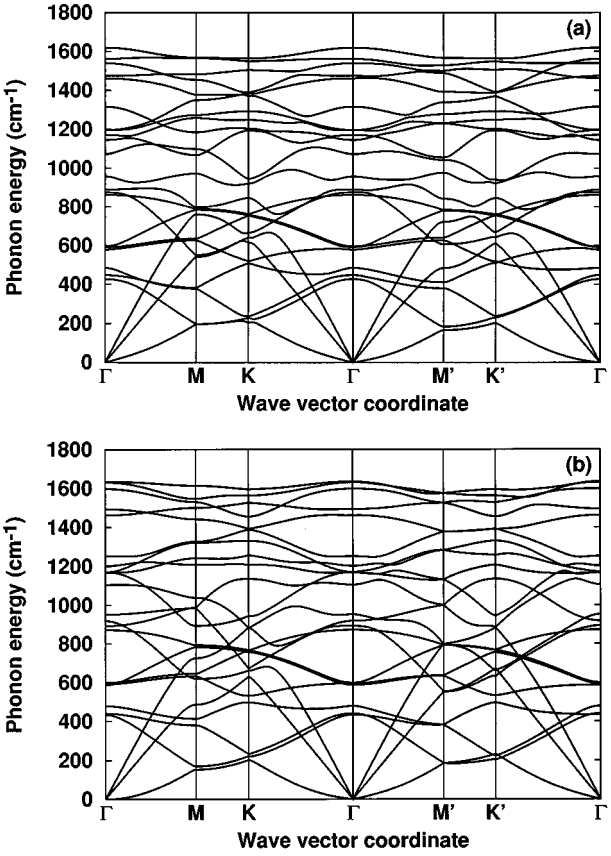

FIG. 10. The calculated phonon dispersion relations of the homogeneous BC_2N systems: (a) for model I and (b) for model II, where the Brillouin zone is given in Fig. 6.

dispersiveless branch causes the above-mentioned characteristic peak structure of model I in Fig. 5.

The calculated phonon dispersion relations of models I and II in Fig. 10 show roughly similar branches, in spite of the existence of the dispersiveless branch of model I. We have calculated the dispersion relations of the other models in Fig. 1, and confirmed that every model has dispersion curves similar to those of monolayer graphite, although degeneracies are broken in BC_2N systems by their structural symmetries. This result represents that the main characteristic of the dispersion relations of BC_2N systems is attributed to their honeycomb lattices, and the differences in atomic arrangements do not exert an influence strong enough to cause drastic changes in the dispersion curves, which is reflected in their total DOS spectra given in Fig. 5. The partial DOS spectra in Fig. 8, however, show the characteristic peak structures depending on the intralayer atomic arrangements as mentioned in Sec. IV A 1. From this result, it is expected that the vibrational modes of models I–V have different atomic displacements, and this is discussed in the next subsection.

3. Vibrational modes

In order to analyze the vibrational modes of the homogeneous BC_2N systems in more detail, some vibrational vectors of models I and II at the Γ point are drawn in Fig. 11. In monolayer BC_2N systems, almost all of the vibrational modes at the Γ point are both Raman active and IR active,

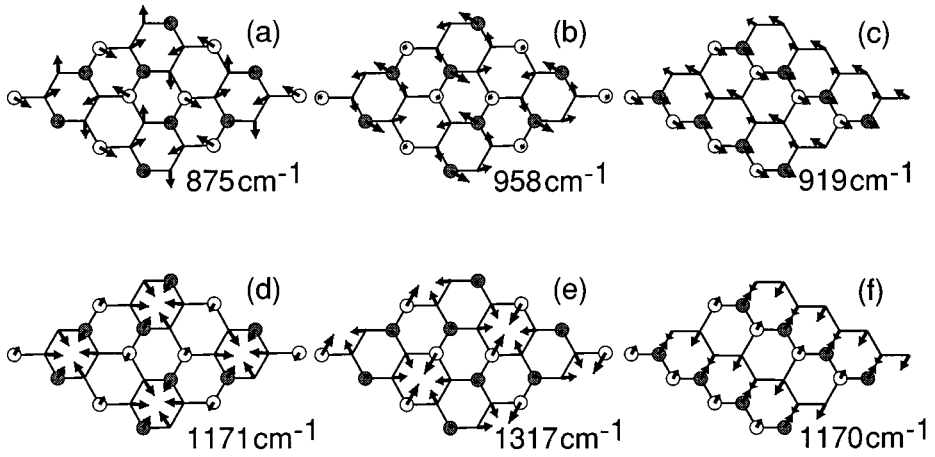

FIG. 11. The obtained vibrational modes of the homogeneous BC_2N systems at the Γ point: (a), (b), (d), and (e) for model I, and (c) and (f) for model II. See text for details.

because of their low structural symmetries. By considering the folding of BZ's, it is possible to relate the BZ's of BC_2N systems with $n\times m$ unit cells to the BZ of monolayer graphite with the 1×1 unit cell. In Fig. 11, all six vibrational modes are related to the normal modes of monolayer graphite at the M point, and the three of them drawn in the upper row [Figs. 11(a)–11(c)] and the other three drawn in the lower row [Figs. 11(d)–11(f)] are derived from the TA and the LA modes, respectively. The calculated phonon frequencies of these in-plane TA and LA modes of monolayer graphite at the M point are 954 and 1192 cm^{-1}, respectively, and they show almost the same atomic displacements as those of model II given in Figs. 11(c) and 11(f). This means, in other words, that the normal modes of model II at the Γ point have the vibrational vectors which correspond to slightly modified ones of graphite. In Fig. 11(c), parallel -C-C- and -B-N- chains are shearing without changing the form of their own zigzag chains, and in Fig. 11(f), B-C and C-N bonds connecting -C-C- and -B-N- chains are stretching also without changing the form of the zigzag chains. In these normal modes of model II, rotational symmetries which are conserved in monolayer graphite (the point group is C_{6v}) have disappeared, because model II has the mirror symmetry only. In contrast to these quasi-one-dimensional vibrational modes of model II, model I has the vibrational modes in which six-membered rings are mainly vibrating as follows: in Figs. 11(a) and 11(b), six-membered rings consisting of four C atoms and two B or N atoms are twisting, and in Figs. 11(d) and 11(e), the same six-membered rings are breathing. In particular, Fig. 11(b) represents the normal mode at the Γ point in the above-mentioned dispersiveless branch of model I. Such twisting and breathing modes never appear in the normal modes of model II at the Γ point, because the 2×1 unit cell of model II cannot include the whole six-membered ring. The same situation is also seen in models III and IV, and in this case -B-C- and -C-N- chains play the same role as -C-C- and -B-N- chains in model II. Since the point group of model I is C_{2v}, the rotational symmetry is conserved in the above-mentioned twisting and breathing modes. Like model I, model V has also the 2×2 unit cell, and thus there are some normal modes at the Γ point which correspond to the twisting and the breathing modes. These normal modes of model V, however, have no symmetry operations because of its low structural symmetry. In Figs. 11(a)–11(c) which are related to the TA mode of monolayer graphite, the bond bending energy makes a larger contribution than the bond stretching one. On the other hand, in Figs. 11(d)–11(f) which are related to the LA mode of monolayer graphite, the bond stretching energy becomes more dominant. As a result, the vibrational modes given in Figs. 11(a)–11(c) have intermediate frequencies of about 900 cm^{-1}.

Although both Figs. 11(a) and 11(b) represent the twisting modes, their calculated phonon frequencies (875 and 958 cm^{-1}) have a large difference of about 80 cm^{-1}, and a larger difference is seen between Figs. 11(d) and 11(e) which represent the breathing modes (1171 and 1317 cm^{-1}). According to Table I, the force constants relating to N atoms are larger than those relating to B atoms, for all terms in Eq. (1). From this viewpoint, it is possible to qualitatively explain the above-mentioned differences in the calculated phonon frequencies of model I. First, in the twisting modes given in Figs. 11(a) and 11(b), bond angles whose center atoms compose the twisting six-membered rings are bending, so that the normal mode shown in Fig. 11(b), in which the six-membered rings containing N atoms are twisting, has higher frequency than that in Fig. 11(a). Secondly, in the breathing modes given in Figs. 11(d) and 11(e), bonds which connect the breathing six-membered rings are stretching, so that the normal mode shown in Fig. 11(e), in which the six-membered rings containing B atoms are breathing and these rings are connected by B-N and C-N bonds, has higher frequency than that in Fig. 11(d). These indicate that there are large splits between the vibrational modes of model I caused by the difference between the force constants of B and N atoms. In fact, the dispersiveless branch whose normal mode at the Γ point is given in Fig. 11(b) arises in the dispersion relation of model I. It has been ascertained that other branches of this model also show such largely split modes. As mentioned above, model V also has twistinglike and breathinglike modes at the Γ point. This model, however, has the almost random atomic arrangement, and thus there are no characteristic six-membered rings and four different kinds of rings per unit cell show similar force constants. As a result, splits of the vibrational modes are small in model V, and its phonon DOS spectrum does not have any distinct peaks as compared with model I in Fig. 5.

The phonon dispersion relations of monolayer graphite and h-BN have a double degeneracy at the Γ point as shown

TABLE II. Calculated phonon frequencies at the Γ point of the homogeneous BC_2N systems. Symbols ω_{st} and ω_{sh} show the frequencies of the stretching and shearing modes, respectively.

Model	Phonon frequencies (cm^{-1})		
	ω_{st}	ω_{sh}	$\omega_{sh}-\omega_{st}$
I	1475	1462	−13
II	1463	1494	31
III	1384	1459	75
IV	1407	1474	67
V	1440	1482	42

in Fig. 4. These degenerated modes in the monolayered model relate to Raman-active E_{2g} mode and IR-active E_{1u} mode in three-dimensional crystal graphite and *h*-BN. The calculated frequencies of the degenerated modes of monolayer graphite and *h*-BN are 1563 and 1444 cm^{-1}, respectively. In monolayer BC_2N systems, these degenerated modes split into two levels at the Γ point. The calculated phonon frequencies of the split modes of models I–V are listed in Table II. The split modes of these five models have vibrational vectors similar to the degenerated modes of graphite sheet. The vibrational vectors of model II are shown in Fig. 12. Parallel -C-C- and -B-N- chains are stretching and shearing in Figs. 12(a) and 12(b), respectively, with changing the form of their own zigzag chains. Concerning the other models in Fig. 1, -B-C-N-C- chains in model I and -B-C- and -C-N- chains in models III and IV are similarly stretching or shearing in their split modes. In models I–V with the two-dimensional crystal structures, these stretching and shearing modes are both Raman active and IR active, except for the shearing mode of model I which is only Raman active. In Fig. 12, the split between the two normal modes of model II is caused by the existence of two kinds of zigzag chains: -C-C- and -B-N-. From this argument, it can be considered that the amount of the split in each model is qualitatively determined by the difference in the force constants between their two zigzag chains: First, in the split modes of models III and IV, parallel -B-C- and -C-N- chains are stretching or shearing like -C-C- and -B-N- chains in Fig. 12. According to Table I, the force constants for the bond stretching energy have the largest difference between B-C and C-N bonds ($K_{r_{(1)}}^{BC}$ and $K_{r_{(1)}}^{CN}$). As a result, the calculated phonon frequencies of models III and IV give the second largest and the largest splits in Table II, respectively. Secondly, in the split modes of model II, -C-C- and -B-N- chains are vibrating as shown in Fig. 12. Since the force constants of C-C and B-N bonds ($K_{r_{(1)}}^{CC}$ and $K_{r_{(1)}}^{BN}$) have close values, the split of model II is smaller than that of models III and IV. Lastly, in the split modes of model I, two equivalent -B-C-N-C- chains are stretching or shearing like -C-C- and -B-N- chains in Fig. 12, and thus model I shows the smallest split in Table II. We have checked that dip structures at about 1430 cm^{-1} in the total DOS spectra of models III and IV given in Fig. 5 are related to their large splits. It is possible to distinguish between the homogeneous BC_2N systems by analyzing these split modes.

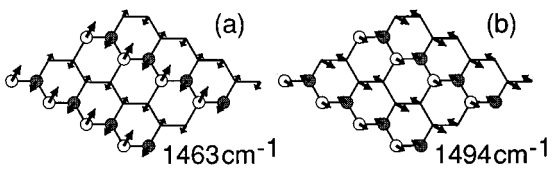

FIG. 12. The obtained vibrational modes of model II at the Γ point, (a) for the stretching mode and (b) for the shearing mode. These two modes correspond to the degenerated modes of graphite at the Γ point. See text for details.

The Raman spectrum of BC_2N has been observed quite recently, and it has two peaks at about 1350 and 1530 cm^{-1}.[15] Unfortunately, it is difficult to discuss the origin of these peaks adequately, because of the lack of high crystallinity in the sample. As for model II which is regarded as the most stable structure among the homogeneous BC_2N, its Raman-active modes in the higher energy region would be separated into three groups by phonon frequency: their calculated frequencies are about 1170, 1480, and 1640 cm^{-1}, where the normal mode given in Fig. 11(f) and the two normal modes given in Fig. 12 belong to the first and the second groups, respectively. There is a possibility that two of these three groups have been observed in the above-mentioned Raman scattering measurement, and in this case, one more peak or shoulder structure would be observed in Raman spectra. On the other hand, it seems that the present experimental data imply the existence of domains segregated into graphitelike and *h*-BN-like regions, because the observed Raman spectra of graphite and *h*-BN have peaks at 1581 and 1366 cm^{-1}, respectively.[11,14] In order to investigate the contribution from such domains, the vibrational properties of the segregated BC_2N systems are presented in the next subsection.

B. Segregated systems

First, we calculated the lattice vibrations of the largely segregated BC_2N systems shown in Fig. 2 whose segregated domains contain 96 atoms in the case of the island pattern. The obtained phonon DOS spectra of the striped and the island patterns are given in Fig. 13. These spectra have been calculated with 97 **q** points in the whole BZ for the 12×8 unit cell, and each vibrational level has been broadened with Gaussian functions of the full width at half maximum of 16.7 cm^{-1}. The superposition of the spectra of graphite and *h*-BN sheets is also shown in Fig. 13. In this figure, the phonon DOS spectra of the segregated BC_2N systems are accurately described by the superposed spectrum of graphite and *h*-BN sheets. There is no meaningful difference between the spectra of the striped and the island patterns, and both spectra show the sharp peak at 1600 cm^{-1} and the shoulder structure at 1680 cm^{-1}, which are contributed by graphitelike and *h*-BN-like networks, respectively, as mentioned in Sec. IV A 1. From these results, it has been concluded that the segregated BC_2N systems given in Fig. 2 have already realized a macroscopic phase separation into graphitelike and *h*-BN-like regions from the viewpoint of the lattice vibration.

Next, in order to ascertain the influence of the segregated domain size, we have investigated the lattice vibrations of the segregated BC_2N systems whose domain size is smaller than that in Fig. 2. Their crystal structures are given in Fig.

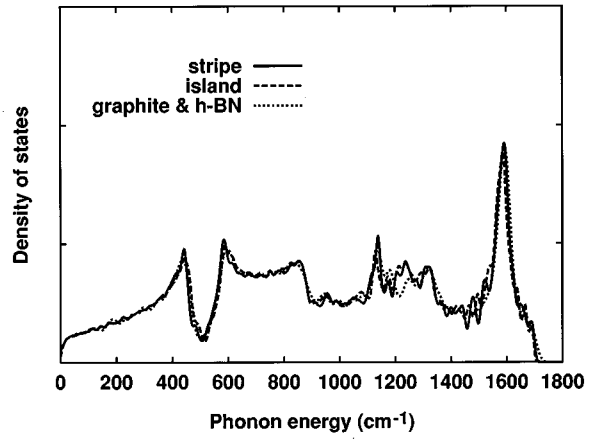

FIG. 13. The calculated phonon DOS spectra of the segregated BC_2N systems given in Fig. 2. Solid and dashed lines show the spectra of the striped and the island patterns, respectively, and dotted line shows the superposed DOS spectrum of monolayer graphite and *h*-BN.

3, and each segregated domain contains 24 atoms in the island pattern. The calculated phonon DOS spectra of these segregated systems are shown in Fig. 14, together with the superposed spectrum of graphite and *h*-BN sheets. In this case, each DOS spectrum has been calculated with 601 **q** points in the whole BZ for the 6×4 unit cell. In Fig. 14, the phonon spectra of the segregated systems are also in fairly good agreement with the superposed spectrum, although some peaks arise around 1200 cm^{-1} as compared with Fig. 13. As mentioned later, these peaks are attributed to the vibrations of atoms which are located in the boundaries between domains. Considering additionally that model II in Fig. 1 corresponds to the striped pattern with the narrowest width and its phonon DOS spectrum given in Fig. 5 cannot be explained by the superposed spectrum of graphite and *h*-BN sheets any longer, it is expected that BC_2N systems whose segregated domains contain dozens of atoms have the

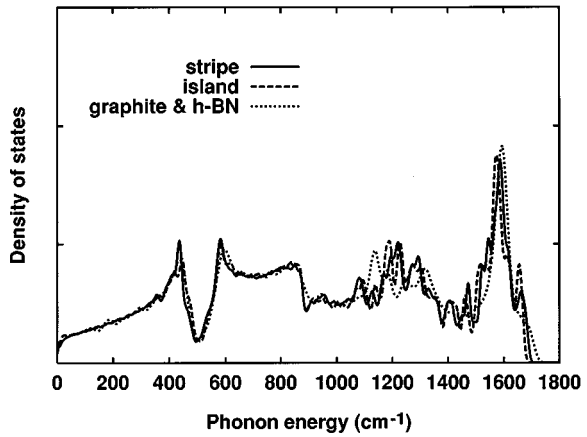

FIG. 14. The calculated phonon DOS spectra of the segregated BC_2N systems given in Fig. 3. Solid and dashed lines show the spectra of the striped and the island patterns, respectively, and dotted line shows the superposed DOS spectrum of monolayer graphite and *h*-BN.

critical domain size between the homogeneous and the segregated BC_2N systems from the viewpoint of the lattice vibration.

In order to investigate the contribution from B-C and C-N bonds which are located in the boundaries between graphitelike and *h*-BN-like regions, we have calculated the partial DOS spectra for two types of atoms, which are positioned in the center of domains and in the boundaries of domains. Concerning both the segregated BC_2N systems given in Figs. 2 and 3, the calculated partial DOS spectra for the atoms located in the center of domains have almost the same peak structures as their total DOS spectra (Figs. 13 and 14) in the whole energy region. However, in the partial DOS spectra for the atoms located in the boundaries, the intensity of the sharp peak at 1600 cm^{-1} decreases and the intensity of some peaks around 1200 cm^{-1} increases as compared with their total DOS spectra. As a result, these partial DOS spectra show peak structures which are quite similar to the total DOS spectra of the homogeneous systems given in Fig. 5. In order to determine whether or not segregated domains exist in BC_2N systems, it is available to compare the intensity of these two peak structures at about 1200 and 1600 cm^{-1} in the total DOS spectra.

We have investigated the normal modes at the Γ point of the striped pattern given in Fig. 3(a). This result implies that the vibrational modes of the segregated BC_2N systems could be roughly classified into three types: in vibrational modes belonging to the first type, all atoms are vibrating independently of the existence of graphitelike and *h*-BN-like regions. On the other hand, in vibrational modes belonging to the second and the third types, atoms in graphitelike region and in *h*-BN-like region are mainly vibrating, respectively. These three types of vibrational modes in the segregated systems are explained by the difference between the lattice vibrations of graphite and *h*-BN. The phonon dispersion relations of monolayer graphite and *h*-BN have similar dispersion curves in the lower energy region. However, in the higher energy region above 1200 cm^{-1}, the dispersion curves of these two materials have different vibrational energies. It has been found that the vibrational modes belonging to the first type are derived from those of graphite and *h*-BN sheets with almost the same frequencies, and the vibrational modes belonging to the second and the third types are derived from those of graphite and *h*-BN sheets which have different frequencies. Thus the phonon DOS spectra of the segregated BC_2N systems can be described by the simple superposition of the spectra of graphite and *h*-BN sheets.

V. CONCLUSIONS

In this paper, we have presented the calculated results for the lattice vibrations of a layered material, BC_2N, and investigated comprehensively the dependence of its vibrational properties on the intralayer atomic arrangements. Since there are huge polymorphic structures of BC_2N, concerning various structural models, their phonon DOS spectra, phonon dispersion relations, and vibrational modes have been compared and analyzed in detail. As the interatomic potential of BC_2N, the generalized valence-force field model is adopted in this study, and its force constants are determined from *ab initio* total energy calculations based on the Hartree-Fock method.

First, the vibrational properties of the homogeneous BC_2N systems have been investigated. In these homogeneous systems, the three elements (B, C, and N) are positioned with the relatively well-mixed arrangements. It has been found that, although the calculated total DOS spectra of models I–V are roughly similar, their partial DOS spectra for the individual atom types have different peak structures depending on the intralayer atomic arrangements. This fact reflects that the vibrational modes of each structural model show characteristic atomic displacements. In particular, model I with the highest structural symmetry has the twisting and the breathing modes at the Γ point in which six-membered rings are mainly vibrating. As compared with these modes, models II–IV have the quasi-one-dimensional vibrational modes at the Γ point in which parallel zigzag chains are stretching or shearing. Based on the numerical results in this study, the lattice vibrations of the homogeneous BC_2N systems would be separated into three parts by vibrational energy: first, in the lower energy region below about 900 cm^{-1}, the phonon DOS spectra have little dependence on the intralayer atomic arrangements, and all structural models show almost the same peak structures. This is due to the fact that the phonon spectra in this energy region are mainly attributed to the vibrational modes with out-of-plane displacement vectors. Next, in the intermediate energy region between about 900 and 1000 cm^{-1}, some vibrational modes such as the twisting modes of model I become obvious, because the bond bending modes are dominant in this energy region as compared with the bond stretching modes. Last, in the higher energy region above 1000 cm^{-1}, the peak structures in the phonon DOS spectra are qualitatively explained by weighted superpositions of the spectra of monolayer graphite, *h*-BN, *h*-BC, and *h*-CN. This suggests that the vibrational properties of BC_2N systems in the higher energy region are represented by the kind and the number of chemical bonds, which is consistent with the fact that vibrational modes in this energy region are determined mainly by the bond stretching modes.

Secondly, the vibrational properties of the segregated BC_2N systems have been investigated. These systems show the phase separation into graphitelike and *h*-BN-like regions. There is expected to be such a phase separation in BC_2N systems from the viewpoint of the bond energy accounting. In contrast to the homogeneous systems, the phonon DOS spectra of the segregated systems can be described by the superposition of the spectra of monolayer graphite and *h*-BN. If segregated domains contain more than dozens of atoms, their phonon DOS spectra have the same peak structures as those of the superposed spectrum in a whole energy region. It is possible to distinguish between the homogeneous and the segregated BC_2N systems based on their lattice vibrations.

In this study, it has been found that the vibrational modes of BC_2N in the higher energy region are sensitively influenced by the intralayer atomic arrangements. There is a conceivable possibility of determining the polymorphic structures of this material by using experimental tools for the vibrational properties. Synthesis of high quality samples of BC_2N is required, and, using such sample, it would be interesting to ascertain which types of phonon spectra of BC_2N could be measured experimentally by Raman scattering, IR absorption, and/or inelastic neutron scattering measurements. This work is now in progress and will be reported in elsewhere. Furthermore, the finite temperature effect is also interesting from the viewpoint of the relation between the structural stability and the lattice vibrations of BC_2N systems, which is an open problem for a future study.

ACKNOWLEDGMENTS

We would like to thank K. Ando, K. Mizushima, and M. O. Watanabe of Toshiba Corporation for stimulating discussion. We are grateful to Y. Miyamoto for sending us a preprint of Ref. 7 prior to publication.

[1] R. B. Kaner, J. Kouvetakis, C. E. Warble, M. L. Sattler, and N. Bartlett, Mater. Res. Bull. **22**, 399 (1987).
[2] J. Kouvetakis, T. Sasaki, C. Shen, R. Hagiwara, M. Lerner, K. M. Krishnan, and N. Bartlett, Synth. Metals **34**, 1 (1989).
[3] A. Y. Liu, R. M. Wentzcovitch, and M. L. Cohen, Phys. Rev. B **39**, 1760 (1989).
[4] H. Nozaki and S. Itoh, J. Phys. Chem. Solids **57**, 41 (1996).
[5] S. Itoh and H. Nozaki, in *Proceedings of 22nd International Conference on the Physics of Semiconductors*, edited by David J. Lockwood (World Scientific, Singapore, 1995), pp. 145–148.
[6] H. Nozaki and S. Itoh, Physica B (to be published).
[7] Y. Miyamoto, M. L. Cohen, and S. G. Louie, Phys. Rev. B **52**, 14 971 (1995).
[8] S. Itoh and H. Nozaki (unpublished).
[9] C. Oshima, T. Aizawa, R. Souda, Y. Ishizawa, and Y. Sumiyoshi, Solid State Commun. **65**, 1601 (1988).
[10] J. L. Wilkes, R. E. Palmer, and R. F. Willis, J. Electron Spectrosc. Relat. Phenom. **44**, 355 (1987).
[11] R. J. Nemanich, G. Lucovsky, and S. A. Solin, Mater. Sci. Eng. **31**, 157 (1977).
[12] R. J. Nemanich, G. Lucovsky, and S. A. Solin, Solid State Commun. **23**, 117 (1977).
[13] S. Jäger, K. Bewilogua, and C.-P. Klages, Thin Solid Films **245**, 50 (1994).
[14] R. J. Nemanich, S. A. Solin, and R. M. Martin, Phys. Rev. B **23**, 6348 (1981).
[15] M. O. Watanabe (private communication).